ChemComm

Accepted Manuscript

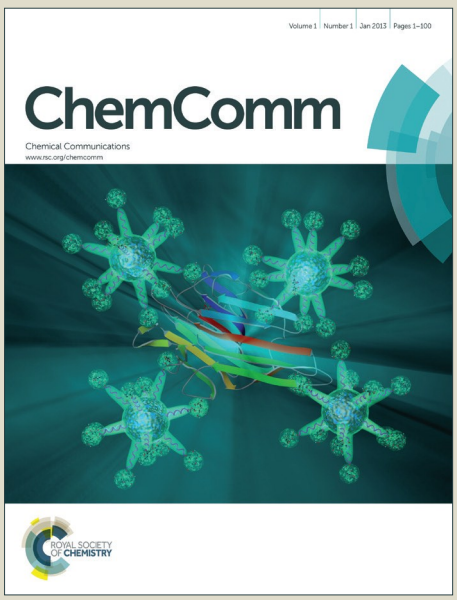

ROYAL SOCIETY OF CHEMISTRY

www.rsc.org/chemcomm

ChemComm

COMMUNICATION

Access to side-chain carbon information in deuterated solids under fast MAS through non-rotor-synchronized mixing

Received 00th January 20xx,
Accepted 00th January 20xx

DOI: 10.1039/x0xx00000x

www.rsc.org/

Natalia Kulminskaya(a)#, Suresh Kumar Vasa(a)#, Karin Giller(a), Stefan Becker(a), Ann Kwan(b), Margaret Sunde(b), Rasmus Linser(a)*

We demonstrate the accessibility of aliphatic ^{13}C side chain chemical shift sets for solid-state NMR despite perdeuteration and fast MAS using isotropic, non-rotor-synchronized ^{13}C-^{13}C mixing. Combined with amide proton detection, we unambiguously and sensitively detect whole side chain to backbone correlations for two proteins using around 1 mg of sample.

A fundamental step for analysis of structure and dynamics in proteins by NMR spectroscopy is resonance assignment for the different nuclei. Countless types of multidimensional NMR experiments have been developed for isotopically labeled proteins, typically with the focus on ^{13}C and ^{15}N nuclei in the solid-state. Backbone chemical shifts deliver important information about the secondary structure, molecular packing of the protein, mobility and many other parameters. Side chain chemical shifts, on the other hand, provide equally important information specific for the residue type and play an essential role in reporting amino acid interactions with neighboring amino acids, other proteins, small molecules, and lipids or water. Moreover, side-chain chemical shifts are also sensitive to conformational changes of the protein. In particular, side-chain dihedral angles χ_i can be defined from chemical shifts and can be used in structure calculation of the protein.[1-3] Exploitation of carbon side chain chemical shifts has proved fundamental in solid-state NMR.[4-6] One of the crucial building blocks of such experiments is the mixing of magnetization among side chain nuclei, which is elicited mostly by proton-driven spin diffusion PDSD [7], dipolar-assisted rotational resonance mixing DARR [8], or other schemes exploiting the strong proton-dipolar coupling network. Such mixing schemes are crucial for residue type identification in the course of protein assignment and for structural information from side chain carbon-carbon through-space correlations.

Proton-detected solid-state NMR on the other hand has been a rapidly expanding approach having grown to a worldwide standard recently.[9-13] In conjunction with extensive ^{2}H labeling (perdeuteration), proton-detected solid-state NMR now enables solution NMR-like correlations[14-16]. In presence of "ultra-fast" Magic-Angle Spinning (using 1.3 mm rotors or smaller) and 100% back-exchange of labile protons, proton-detected solid-state NMR represents an eight-fold increase in sensitivity per amount of protein compared with ^{13}C detection.[17] The sensitivity advantages are even increased in combination with paramagnetic relaxation enhancement, which can overcome slow ^{1}H and ^{13}C longitudinal T_1 relaxation and enable fast recycling of the experiments in the absence of high-power decoupling.[18, 19] Thus, proton detection in combination with ultra-fast MAS becomes especially useful for proteins which are difficult to produce in large amounts.[20-22]

Unfortunately, the price to pay for overcoming the hurdles of a strong proton-proton dipolar-coupling network by fast spinning and particularly by deuteration is the inaccessibility of "proton-dependent" conventional mixing schemes like DARR,[8] PDSD,[7] or CHHC.[23] Utilization of deuterons has been suggested as a potential remedy[24, 25] if an additional (fourth) deuterium channel is available. Radio-frequency-driven recoupling RFDR,[26] HORROR,[27] and symmetry-based sequences[28] can be an option for replacing PDSD and DARR experiments. However, under fast MAS, such sequences can face limitations in terms of maximum radio frequency power that can be tolerated by the sample. This becomes increasingly problematic as spinning speeds are increased. Thus, the mentioned elements tend to be limited to short mixing times, which significantly reduces the available options for getting the long-range correlations necessary for identifying side chain resonance sets. As demonstrated by studies employing low-power variants of the established recoupling sequences,[29-32] there is a growing incentive to find homonuclear mixing schemes amenable for the rapidly increasing MAS rates.

Here we demonstrate the effectiveness of an isotropic homonuclear mixing scheme from solution NMR, MOCCA,[33-35] for amide proton-detected NMR approaches at sample spinning f

[a] Max-Planck Institute for Biophysical Chemistry, Department NMR-Based Structural Biology, Am Fassberg 11, 37077 Göttingen
[b] School of Medical Sciences and School of Molecular Bioscience, University of Sydney, Sydney, Australia
# Authors contributed equally to this work.
* Corresponding author: rali@nmr.mpibpc.mpg.de
Electronic Supplementary Information (ESI) available: [details of any supplementary information available should be included here]. See DOI: 10.1039/x0xx00000x

55 kHz. We have previously demonstrated the feasibility of MOCCA mixing for traditional 2D carbon-carbon correlations for partially (30%) back-exchanged, deuterated proteins at moderate spinning speed.[36]

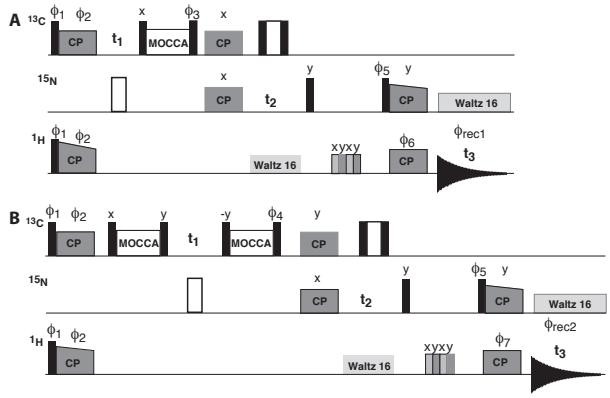

Figure 1. (A) Schematic representation of the pulse sequence for the ^{1}H-detected 3D (H)CX(CA)NH experiments with one or two ^{13}C-^{13}C isotopic mixing building blocks. Narrow black and white open bars represent hard 90 and 180-degree pulses, respectively. The ^{1}H-^{13}C CP contact time was set to 2100 µs. For the ^{15}N-^{13}CA CP, rf fields were set to 36.7 kHz and 24.4 kHz on ^{13}C and ^{15}N, respectively, with a contact time of 9 ms. For the ^{15}N-^{1}H CP, rf fields of 54.23 kHz and 14.4 kHz were used with a contact time of 300 µs. The phase cycles employed are: ϕ_1 = x, -x, ϕ_2 = y, -y, ϕ_3 = y, y, y, y,-y,-y,-y,-y, ϕ_4 = x, x, x, x, –x, –x, –x, –x, ϕ_5 = x,x,-x,-x, ϕ_6 = ϕ_7 =x, x, x, x, x, x, x, x, -x, -x, -x, -x, -x, -x, -x, -x, ϕ_{12} = x, x, x, x, -x, -x, -x, -x, $\phi_{rec1,2}$ = x,-x,-x, x, -x, x, x, -x, -x, x, x, -x, x, -x, x, -x.

Isotropic ^{13}C-^{13}C mixing in the context of proton-detected NMR at "ultra-fast" spinning (rotor diameters of 1.3 mm and smaller) enables us to obtain proton-detected side-chain carbon spectra on uniformly ^{15}N, ^{13}C, ^{2}H-labeled proteins back-exchanged in 100% H_2O:[17] For methods development, we employed the SH3 domain of α-spectrin.[4] We then applied the approach to obtain side chain assignments from functional amyloid rodlets composed of a fungal hydrophobin protein[37-39]. Hydrophobin rodlets are characterized by a structured core together with substantial sample heterogeneity.[40] In the absence of a dipolar-coupling network and high magnetic field at ultra-fast MAS, the solution NMR sequence proves capable of establishing connectivites between the protein backbone and the entire sets of side chain carbon resonances in 3D CCCANH-type experiments, without compromising sample integrity by sample heating. Although heterogeneous samples usually tend to require 4D and 5D experimental setup to overcome the resonance overlap, here near-complete aliphatic side-chain resonance assignments could be obtained using a single 3D CCCANH experiment.

First, we tailored MOCCA conditions and optimized the CO-PORADE approach[41] for ultra-fast MAS. Secondly, we used MOCCA as a building block for 3D CCCANH experiments to obtain residue-specific side-chain chemical-shift information. Depending on the sample-dependent doping characteristics, see below, we could use either one mixing block (before frequency encoding, Fig. 1A) or two mixing blocks (before and after frequency encoding, Fig. 1B) to access intra-residual connectivites in the absence of side-chain protons.

MOCCA mixing involves optimization of two parameters, the 180° pulse length and the delay between the pulses (Fig. 1 and S1. First, we optimized the 180° pulse length using RFD conditions without phase cycling the RFDR pulse. (See the SI for details.) In the next step, we evaluated the performance of MOCCA at different mixing times and compared with RFDR an example of a well-established rotor-synchronized r coupling sequence as shown for exemplary residues in Fig. 2 and S3 (SI). It is evident from the figure that we could use longer mixing times amounting to similar amounts of ener y dissipated into the probe with MOCCA in comparison to RFDR. Although the RFDR buildup behavior is slightly faster than MOCCA, the latter performs well with mixing times as long 7 ms. This enables relayed transfers providing many high intensity cross peaks with improved performance particular for 2- or 3- bond transfers (Figs. 1A and S3). A comparison of 2D correlation spectra with extensive mixing times for bo RFDR and MOCCA is shown in Fig. S4. Taking into account the feasibility of long mixing times using MOCCA with very low longitudinal magnetization loss (Fig. S5), the approach might be useful for other applications like long-range magnetiza transfer through ^{3}J couplings or similar. In contrast, carbonyl and aromatic buildup is less efficient than with RFDR. Thi might be due to the faster buildup for RFDR, which wou mean sufficient mixing even for partial DD introduction in the presence of off-resonance effects. Similar observations a made with moderate MAS up to 25 kHz with 30% proto backexchanged samples.[36]

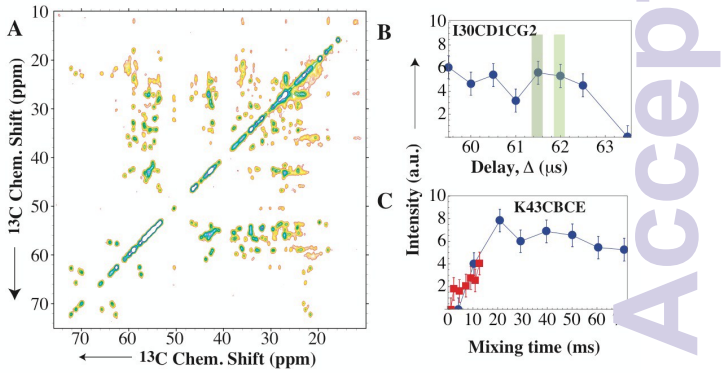

Figure 2. (A). 2D ^{13}C-^{13}C correlation experiments using MOCCA with the COPORADE approach[41] (see Fig. S10), highlighting aliphatic side-chain carbons of the SH3 domain at 55.5 kHz MAS. The experiment was recorded with a MOCCA isotropic mixing time of ms and a total experimental time of 3 hours. (B) 2D experimental optimization of t delay, Δ, between the 180° degree pulses of MOCCA for efficient multiple-bond trans fer. The total experimental time for each 2D experiment was 3 hours. The optim experimental delays are shown in dark and light green colors. (C) Experimental build- p curves of signal intensity for MOCCA (blue) and RFDR (red), adhering to similar limi tions for power dissipation: Examples of ^{13}C-^{13}C transfer efficiency for three-bon magnetization transfer. The radiofrequency pulse strength for RFDR and MOCCA w s set to 59.5 kHz. The 180-degree pulse was set 8.37 µs and the delay between the pulses, Δ, was set to 61.5 µs and 9.63 µs for MOCCA and RFDR, respectively.

After determining the optimized conditions for MOCCA at fas MAS, we incorporated this mixing sequence into a 3D CCCAN (or (H)CX(CA)NH) experiment in order to assign side-cha resonances in conjunction with proton detection for increase resolution and sensitivity. Here, we used the COPORADE ap proach, which enables both effective backbone and sidecha carbon polarization in deuterated samples, with paramagneti

doping for fast relaxation and shortened recycle delays. Corresponding 3D sequences are shown in Figs. 1A and B using one or two mixing blocks, respectively. For a crystalline sample like SH3, paramagnetic chelates can travel throughout the protein lattice, and it has been shown that doping very effectively reduces the spin-lattice relaxation times of ^{1}H and ^{13}C.[19] The resulting relaxation enhancement for both nuclei ensures high sensitivity with fast repetition rates. For this kind of samples, abundant side-chain ^{13}C polarization even for those carbons that are too far away from H^N to be polarized by H-C CP has been shown to be available in the indirect dimensions with one mixing block.[41] For a 3D (H)CX(CA)NH spectrum recorded on the SH3 domain, representative strips are depicted in Fig. 3. The strips demonstrate the highly resolved side chain ^{13}C correlations dispersed by their amide ^{1}H and ^{15}N chemical shifts.

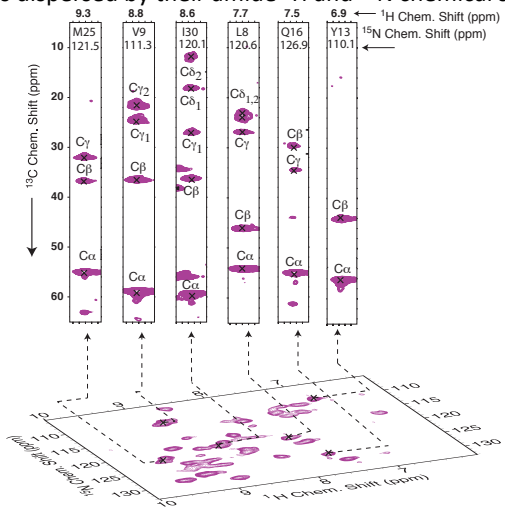

Figure 3. Illustrative strip plot from a ^{1}H-detected 3D (H)CX(CA)NH experiment, yielding side chain to backbone correlations for uniformly-labelled ^{15}N, ^{13}C, ^{2}H SH3 domain (100% proton back exchanged). A 2D HN projection is shown on the bottom. Mixing time applied in the experiment is 32.5 ms.

For many microcrystalline proteins like SH3, good ^{1}H-^{15}N-resolution spectra are obtained, which enables an effective dispersion of side chain ^{13}C strips. By contrast, as expected it is more challenging to study amyloids, where a low amide resolution is found due to sample heterogeneity (see Fig. S10). Here we applied the experimental approach to hydrophobin rodlets. This protein generates a hydrophobic coating on fungal spores, which improves their wettability characteristics.[38, 39] The overall behavior of the rodlet samples is dominated by severe heterogeneity of the sample for both proton- and carbon-detected experiments as shown by Morris et al.[40] and has so far remained a challenge for solid-state NMR characterization. This can be derived from their amide spectral dispersion and sensitivity (see Fig. S10). In addition, a lower overall accessibility of the protein to the paramagnetic agent due to the packing in the fibrillar, amyloid state[18] than in the crystalline state with solvent channels, give rise to large carbon T_1 values despite identical dopant concentrations. Whereas C^{α} can still be sufficiently polarized by H-C CP, the ^{13}C Boltzmann polarization required for side chain carbons distant from H^N at the chosen recycle delay is low. However, we could partially alleviate this problem by inserting an additional MOCCA mixing block before chemical shift encoding (Fig. 1B) to mix proto- polarized C^{α} magnetization into the side chain before the fir- chemical shift evolution. Even though this way we still mai- tain higher C^{α} peaks, we observe an effective increase of id- chain polarization by initial CA-to-CX mixing.

Apart from access to single side chain chemical shifts, th- value of the access to aliphatic carbon resonance sets by MOCCA mixing is apparent from the spectra obtained on th- heterogeneous hydrophobin sample. Fig. 4 shows strips from the 3D (H)CX(CA)NH NMR experiment, effectively overcoming the intrinsic sample heterogeneity in conjunction with the lo- amount of sample required. Overall, using the side chain t- backbone correlation approach, we managed to identify ar- assign individual contributions of many assigned residues t- the HN plane by their side-chain carbon chemical shifts wit- out going to higher spectral dimensions. The side chain sh- effectively help to deconvolve and unambiguously assign the protein despite a lack of HN resolution.

Side-chain carbon shift accessibility is important for determining hydrophobic contacts within protein structures and with other molecules. Side-chain carbon shifts are also sensitive to many factors including tertiary structural contacts, intermolecular contacts, ring currents, as well as rotamer confo- mations. Apart from the possibility of resolving overlapping correlations for assignment purposes as shown for this hydro- phobin rodlet sample, we thus expect manifold applicatio- arising from the accessibility of side chain carbon chemica- shifts in conjunction with the sensitivity provided from proto- detected solid-state NMR studies.

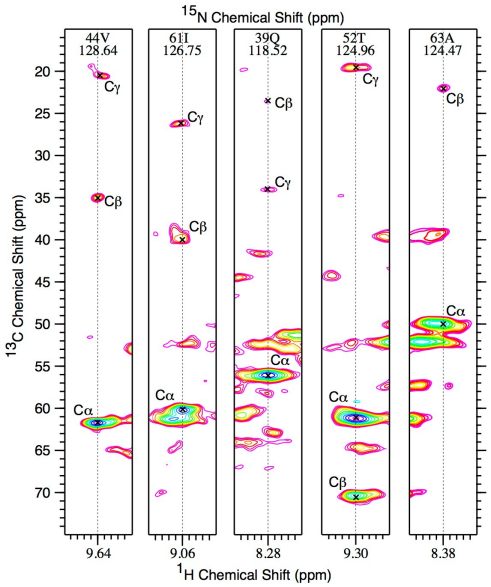

Figure 4. Strip plots from a ^{1}H-detected 3D (H)CX(CA)NH experiment on 100% - exchanged $EAS_{\Delta 15}$ hydrophobin rodlets. All experimental conditions are similar to th- SH3 protein, however relying on out-and-back mixing of C^{α} magnetization, hence t- e low cross-peak-to-diagonal peak ratio. Mixing time is 60.7 ms. The experimental ti- e was around 48 hours. The strip plots of 39Q, 52T, 63A are shown with slightly high- contour levels.

We have shown that by using a non-rotor-synchronized carbon-carbon liquid-state mixing sequence based on *J*-coupling- together with low power requirements, we are able to obtain

amide-resolved proton-detected sidechain-to-backbone correlations despite fast MAS and in the absence of side-chain protons. We demonstrate the sensitive access to side-chain resonances from only 1 mg of protein material for a microcrystalline protein as well as for a functional amyloid known to pose significant hurdles to solid-state NMR due to its inhomogeneity. As a *J*-coupling-based sequence with extremely low duty, MOCCA does not require rotor synchronization, allows long mixing times and multiple-bond transfers without major power dissipation at fast MAS. MOCCA provides access to the sets of side chain carbon shifts from a heterogeneous protein sample in spite of spectral overlap in the HN plane even in three dimensions, strongly facilitating unambiguous resonance assignment and reporting manifold local biophysical parameters.

Acknowledgements

We thank Brigitta Angerstein for technical assistance. RL acknowledges support from the Max-Plank Gesellschaft, from the Deutsche Forschungsgemeinschaft (SFB 803, project A04, and an Emmy Noether fellowship), and the Verband der Chemischen Industrie (VCI) in terms of a Liebig junior group fellowship. We acknowledge Karyn Wilde and Anthony Duff from the Australian and Nuclear Science Organisation for the overexpression of uniformly ^{15}N, ^{13}C, ^{2}H-labeled $EAS_{\Delta 15}$ hydrophobin.

References

1. Y. Shen and A. Bax, *J Biomol NMR*, 2013, **56**, 227-241.
2. R. E. London, B. D. Wingad and G. A. Mueller, *J Am Chem Soc*, 2008, **130**, 11097-11105.
3. M. Hong, T. V. Mishanina and S. D. Cady, *J Am Chem Soc*, 2009, **131**, 7806-7816.
4. F. Castellani, B.-J. van Rossum, A. Diehl, M. Schubert, K. Rehbein and H. Oschkinat, *Nature*, 2002, **420**, 98–102.
5. A. Loquet, N. G. Sgourakis, R. Gupta, K. Giller, D. Riedel, C. Goosmann, C. Griesinger, M. Kolbe, D. Baker, S. Becker and A. Lange, *Nature*, 2012, **486**, 276-279.
6. S. H. Park, B. B. Das, F. Casagrande, Y. Tian, H. J. Nothnagel, M. Chu, H. Kiefer, K. Maier, A. A. De Angelis, F. M. Marassi and S. J. Opella, *Nature*, 2012, **491**, 779-783.
7. N. Bloembergen, *Physica*, 1949, **15**, 386-426.
8. K. Takegoshi, S. Nakamura and T. Terao, *Chem. Phys. Lett.*, 2001, **344**, 631-637.
9. M. J. Knight, A. J. Pell, I. Bertini, I. C. Felli, L. Gonnelli, R. Pierattelli, T. Herrmann, L. Emsley and G. Pintacuda, *Proc. Natl. Acad. Sci. U.S.A.*, 2012, **109**, 11095-11100.
10. V. Agarwal, S. Penzel, K. Szekely, R. Cadalbert, E. Testori, A. Oss, J. Past, A. Samoson, M. Ernst, A. Böckmann and B. H. Meier, *Angew. Chem. Int. Ed.*, 2014, **53**, 12253-12256.
11. P. Ma, J. D. Haller, J. Zajakala, P. Macek, A. C. Sivertsen, D. Willbold, J. Boisbouvier and P. Schanda, *Angew. Chem. Int. Ed.*, 2014, **53**, 4312-4317.
12. S. Asami, J. R. Porter, O. F. Lange and B. Reif, *J. Am. Chem. Soc.*, 2015, **137**, 1094-1100.
13. D. H. Zhou, J. J. Shea, A. J. Nieuwkoop, W. T. Franks, B. J. Wylie, C. Mullen, D. Sandoz and C. M. Rienstra, *Angew. Chem., Int. Ed.*, 2007, **46**, 8380-8383.
14. R. Linser, U. Fink and B. Reif, *J Magn Reson*, 2008, **193**, 89-93.
15. V. Chevelkov, K. Faelber, A. Diehl, U. Heinemann, H. Oschkinat and B. Reif, *J. Biomol. NMR*, 2005, **31**, 295-310.
16. P. Schanda, M. Huber, R. Verel, M. Ernst and B. H. Meier, *Angew. Chem., Int. Ed.*, 2009, **48**, 9322-9325.
17. J. R. Lewandowski, J.-N. Dumez, U. Akbey, S. Lange, L. Emsley and H. Oschkinat, *J. Phys. Chem. Lett.*, 2011, **2**, 2205-2211.
18. N. P. Wickramasinghe, S. Parthasarathy, C. R. Jones, C. Bhardwaj, F. Long, M. Kotecha, S. Mehboob, L. W. M. Fung, J. Past, A. Samoson and Y. Ishii, *Nature methods*, 2009, **6**, 215-218.
19. R. Linser, V. Chevelkov, A. Diehl and B. Reif, *J. Magn. Reson.*, 2007, **189**, 209–216.
20. J. M. Lamley, D. Iuga, C. Öster, H.-J. Sass, M. Rogowski, A. Oss, J. Past, A. Reinhold, S. Grzesiek, A. Samoson and J. R. Lewandowski, *J Am. Chem. Soc.*, 2014, **136**, 16800-16806.
21. R. Linser, B. Bardiaux, S. G. Hyberts, A. H. Kwan, V. K. Morris, M. Sunde and G. Wagner, *J. Am. Chem. Soc.*, 2014, **136**, 11002–11010.
22. S. Wang, S. Parthasarathy, Y. Xiao, Y. Nishiyama, F. Long, I. Matsuda, Y. Endo, T. Nemoto, K. Yamauchi, T. Asakura, M. Takeo, T. Terauchi, M. Kainosho and Y. Ishii, *ChemComm*, 2015, **DOI: 10.1039/c5cc04618a**.
23. A. Lange, K. Seidel, L. Verdier, S. Luca and M. Baldus, *J. Am. Chem. Soc.*, 2003, **125**, 12640–12648.
24. U. Akbey, H. Oschkinat and B. J. van Rossum, *J. Am. Chem. Soc.*, 2009, **131**, 17054-+.
25. Ü. Akbey, F. Camponeschi, B.-J. van Rossum and H. Oschkinat, *ChemPhysChem*, 2011, **12**, 2092-2096.
26. A. E. Bennett, J. H. Ok, R. G. Griffin and S. Vega, *J. Chem. Phys.*, 1992, **96**, 8624-8627.
27. N. C. Nielsen, F. Creuzet, R. G. Griffin and M. H. Levitt, *J. Chem. Phys.*, 1992, **96**, 5668-5677.
28. M. H. Levitt, in *Encyclopedia of Nuclear Magnetic Resonance*, eds. D. M. Grant and R. K. Harris, 2002, vol. 9, pp. 165-196.
29. G. Teymoori, B. Pahari, E. Viswanathan and M. Edén, *Journal of Magnetic Resonance*, 2013, **236**, 31-40.
30. A. B. Nielsen, S. K. Jain and N. C. Nielsen, *Chem. Phys. Lett.*, 2011, **503**, 310-315.
31. C. Herbst, J. Herbst, J. Leppert, O. Ohlenschläger, M. Görlach and R. Ramachandran, *J Biomol NMR*, 2011, **50**, 277-284.
32. P. Bellstedt, C. Herbst, S. Häfner, J. Leppert, M. Görlach and R. R., *J. Biomol. NMR*, 2012, **54**, 325-335.
33. Y. Yoshimura, N. V. Kulminskaya and F. A. Mulder, *J Biomol NMR*, 2015, **61**, 109-121.
34. F. Kramer, W. Peti, C. Griesinger and S. J. Glaser, *J Magn Reson*, 2001, **149**, 58-66.
35. I. C. Felli, R. Pierattelli, S. J. Glaser and B. Luy, *J Biomol NMR*, 2009, **43**, 187-196.
36. N. Kulminskaya, S. K. Vasa, K. Giller, S. Becker and R. Linser, *J. Biomol. NMR*, 2015, **DOI: 10.1007/s10858-015-9980-1**
37. H. A. B. Wösten, O. M. H. Devries and J. G. H. Wessels, *Plant Cell*, 1993, **5**, 1567–1574.
38. M. Sunde, A. H. Kwan, M. D. Templeton, R. E. Beever and J. P. Mackay, *Micron*, 2008, **7**, 773–784.
39. A. H. Y. Kwan, R. D. Winefield, M. Sunde, J. M. Matthews, R. G. Haverkamp, M. D. Templeton and J. P. Mackay, *Proc. Natl Acad. Sci. U.S.A.*, 2006, **103**, 3621-3626.
40. V. K. Morris, R. Linser, K. L. Wilde, A. P. Duff, M. Sunde and A. H. Kwan, *Angew. Chem., Int. Ed.*, 2012, **51**, 12621-12625.
41. R. Linser, *J. Biomol. NMR*, 2011, **51**, 221-226.